A Statistical Analysis on the Dependence of Tropical Cyclone Intensification Rate on the Storm Intensity and Size in the North Atlantic

JING XU

State Key Laboratory of Severe Weather, Chinese Academy of Meteorological Sciences, China Meteorological Administration, Beijing, China

YUQING WANG

International Pacific Research Center, and Department of Atmospheric Sciences, School of Ocean and Earth Science and Technology, University of Hawai'i at Mānoa, Honolulu, Hawaii

(Manuscript received 25 October 2014, in final form 22 December 2014)

ABSTRACT

The dependence of tropical cyclone (TC) intensification rate IR on storm intensity and size was statistically analyzed for North Atlantic TCs during 1988–2012. The results show that IR is positively (negatively) correlated with storm intensity (the maximum sustained near-surface wind speed V_{max}) when V_{max} is below (above) 70–80 knots (kt; 1 kt = 0.51 m s^{-1}), and negatively correlated with storm size in terms of the radius of maximum wind (RMW), the average radius of gale-force wind (AR34), and the outer-core wind skirt parameter DR34 (=AR34 − RMW). The turning point for V_{max} of 70–80 kt is explained as a balance between the potential intensification and the maximum potential intensity (MPI). The highest IR occurs for V_{max} = 80 kt, RMW ≤ 40 km, and AR34 = DR34 = 150 km. The high frequency of occurrence of intensifying TCs occurs for V_{max} ≤ 80 kt and RMW between 20 and 60 km, AR34 ≤ 200 km, and DR34 ≤ 150 km. Rapid intensification (RI) often occurs in a relatively narrow parameter space in storm intensity and both inner- and outer-core sizes. In addition, a theoretical basis for the intensity dependency has also been provided based on a previously constructed simplified dynamical system for TC intensity prediction.

1. Introduction

After the genesis of a tropical cyclone (TC) under favorable environmental conditions, such as high sea surface temperatures (SSTs), weak vertical wind shear, and a deep upper-ocean mixed layer, the storm usually experiences an intensification period before it reaches its mature stage (Gray 1979). These large-scale parameters are important predictors used in operational statistical TC intensity forecast models (DeMaria and Kaplan 1999; DeMaria et al. 2005; DeMaria 2009). However, even though these environmental parameters are included in most operational prediction models, the prediction skill for TC intensity change has remained low compared with that for TC motion (Elsberry et al. 2007, 2013). This is partly due to the fact that TC motion is largely controlled by the large-sale environmental flow while TC intensity change is controlled by an array of scales and their interactions (Wang and Wu 2004; Elsberry et al. 2013).

Among different scales, the potential effect of the TC inner-core size and intensity on its intensification has been recognized for a long time from a theoretical viewpoint (Shapiro and Willoughby 1982; Schubert and Hack 1982; Pendergrass and Willoughby 2009). For example, Shapiro and Willoughby (1982) showed that the response of a balanced TC vortex to a given eyewall heating is a maximum increase in tangential wind inside the RMW, giving rise to a contraction of the eyewall as the TC intensifies. The tangential wind tendency (namely intensification rate IR) was shown to increase as the TC intensity increases. This intensity dependence of IR as a response to a given eyewall heating was later explained in terms of the inertial stability in the inner core by Schubert and Hack (1982). They showed that the inertial stability inside of the radius maximum wind (RMW), which determines the efficiency of warming in the eye and the tangential wind tendency in response to

Corresponding author address: Prof. Yuqing Wang, IPRC/SOEST, P.O. Box 404A, 1680 East–West Rd., Honolulu, HI 96822.
E-mail: yuqing@hawaii.edu

DOI: 10.1175/WAF-D-14-00141.1

diabatic heating in the eyewall, increases as the TC vortex intensifies. Since the inner-core inertial stability is a function of not only the storm intensity but also the inner-core size (such as the RMW) for a given intensity, the above theoretical studies also suggest that the IR could depend on the inner-core size of the TC itself. Previous studies based on balanced dynamics have also shown that diabatic heating inside the RMW is key to the rapid development of a warm core (Vigh and Schubert 2009; Pendergrass and Willoughby 2009) although no explanation has been given to date to address what controls the radial location of eyewall heating relative to the RMW.

Recent observational studies have begun to focus on the potential impact of TC structure on its intensification (Chen et al. 2011; Rogers et al. 2013; Carrasco et al. 2014). Chen et al. (2011) found that compact TCs (either small RMW, or weak outer-core wind, or both) had a higher IR and more frequent rapid intensification (RI) relative to incompact storms over the western North Pacific. Rogers et al. (2013) compared the composite structures of intensifying and quasi-steady TCs based on airborne radar data for the North Atlantic and found that the tangential wind outside the RMW decays with radius more rapidly with eyewall heating located more inside the RMW in intensifying TCs than in quasi-steady TCs. Since slow-decaying tangential wind with radius outside the RMW (incompact TCs) implies high inertial stability in the outer core, this result seems to suggest that high inertial stability in the outer core may reduce the boundary layer inflow and its inward penetration into the eye region. This may prevent convective updrafts and thus eyewall heating from occurring inside the RMW. Therefore, in addition to the inner-core size (such as the RMW), the outer-core size or the radial decaying rate of tangential wind outside the RMW may also be a key factor affecting the TC IR.

Recently, Carrasco et al. (2014) compared three size parameters [RMW, the average 34-knot (kt; 1 kt = 0.51 m s^{-1}) wind radius (AR34), and the radius of the outermost closed isobar (ROCI)] of TCs that underwent RI versus those that are steady state or slowly intensifying over a 24-h period for the North Atlantic TCs during 1990–2010. They found that both RMW and AR34 have the strongest negative correlations with intensity change. A maximum size threshold was shown to exist for both RMW and AR34, above which RI is extremely rare while ROCI (they referred it as a measure of the outer-core size) appears to have little correlation with subsequent IR. They also found that although AR34 is negatively correlated with the subsequent IR, the correlation is weaker than RMW. This seems to be consistent with earlier findings that the inner- and outer-core wind fields vary nearly independently (Merrill 1984; Weatherford and Gray 1988).

In addition to the inner- and outer-core sizes, the initial TC intensity has also been shown to affect the subsequent IR, as inferred from the balanced dynamics mentioned above. Based on the best-track data for the North Atlantic from 1989 to 2006, Kaplan et al. (2010) found that the distribution of RI cases for the 25- and 30-kt IR thresholds was skewed to cases with 35–40-kt initial intensities, and TCs with initial intensities of 65–70 kt were the most likely to satisfy the 35-kt RI threshold. They hypothesized that the former might be a reflection of the tendency for storms that were far away from their maximum potential intensity (MPI) and the latter could be a result that TCs of 65–70-kt intensity were both sufficiently well organized and still far enough from their MPI. Indeed, the initial intensity has been used as a predictor in several operational statistical intensity prediction schemes (e.g., DeMaria et al. 2005; DeMaria 2009). The dependence of the IR on TC intensity will be further examined with longer data records in this study.

The objective of this study is to examine the dependence of the subsequent 24-h IR on the initial TC intensity and its inner- and outer-core sizes based on the best-track data for the North Atlantic basin from 1988 to 2012. The relative importance of the inner- and outer-core sizes on the subsequent IR will also be reexamined quantitatively. The rest of the paper is organized as follows. Section 2 describes the data and methodology used in this study. The results are discussed in section 3. The major findings are summarized in the last section.

2. Data and methodology

The best-track data for Atlantic TCs from the National Hurricane Center (NHC), known as the revised Atlantic hurricane database (HURDAT2), and the Extended Best-Track (EBT) dataset developed by Demuth et al. (2006) for North Atlantic TCs during 1988–2012, were used in this study. HURDAT2 consists of the 6-hourly TC location (latitude, longitude), maximum 1-min-mean sustained surface wind V_{max}, central sea level pressure, and maximum radial extent by quadrant of the 34-kt wind for each TC. The RMW is retrieved from the EBT dataset since it is not included in HURDAT2. All extra- and subtropical transitions and tropical depression stages of TCs and records after landfall were removed from our analysis. A total of 341 TCs were included in this study.

We define IR as an increase in V_{max} over a 24-h period and RI as the top 95th percentile of the overwater 24-h change of TC intensity, which is about 30 kt day^{-1} or greater (Kaplan and DeMaria 2003) for North Atlantic TCs during the studied period. Accordingly, non-RI TCs are defined as having an IR greater than zero but less

than the RI threshold. There are 2634 intensifiers, and among them 373 are RI cases.

Two size parameters, namely RMW and AR34, respectively, referred to as the inner- and outer-core sizes, are considered in this study. As in Carrasco et al. (2014), the AR34 at a given time is the average of nonzero radii of 34-kt surface wind among the four quadrants.[1] We note that this algorithm for AR34 might lead to considerable problems for weak tropical storms. We expect that the overall results would not be significantly affected by the simple algorithm. In addition, the influence of the TC outer-core tangential wind profile on its IR and RI is also examined. The decaying rate of the tangential wind with radius outside the RMW is measured by the width of the ring between RMW and AR34 for a TC, which is referred to as the wind skirt parameter (DR34) in this study. This measure roughly reflects the outer-core size or the compactness of the TC vortex. Note that the estimates of RMW and AR34 might be less accurate for cases without aircraft observations than those with aircraft observations. As a result, we should keep in mind that some uncertainties might exist in both RMW and AR34 in the observations. Nevertheless, the dataset we used is still the best available for us to conduct such a study.

To investigate quantitatively the relationship between TC IR and its initial intensity and various size parameters, the nonparametric regression technique (Green and Silverman 1994) is employed in this study. The regression is assumed to have a form of

$$y_i = f(\mathbf{x}_i) + \varepsilon_i, \tag{1}$$

Where y_i ($i = 1, \ldots, n$) is the ith dependent variable, f is the smoothing function, $\mathbf{x}_i$ represents the d-dimensional covariates, and ε_i is the independent error. The fitting is achieved by minimizing the residual sum of squares subject to a constraint so that the function has a certain level of smoothness (or a roughness penalty),

$$\sum_{i=1}^{n} [y_i - f(x_i)]^2 + \lambda \int [f''(x)]^2 \, dx, \tag{2}$$

for univariate $f(x)$, and

$$\sum_{i=1}^{n} [y_i - f(u_i, v_i)]^2 + \lambda \iint \left[\left(\frac{\partial^2 f}{\partial u^2} \right)^2 + 2 \left(\frac{\partial^2 f}{\partial u \partial v} \right)^2 + \left(\frac{\partial^2 f}{\partial v^2} \right)^2 \right] du \, dv, \tag{3}$$

for bivariate $f(u, v)$, where λ is the parameter controlling the level of smoothness and is estimated by generalized cross validation. The fitted f is a smoothing curve constructed by natural cubic splines for the univariate case (Figs. 1 and 2a), or a smoothing surface constructed by thin plate splines for the bivariate case (Fig. 3). Smoothing surfaces in the analysis are defined on convex hulls, within which the sample data are derived.

3. Results

a. Dependence on storm intensity

Figure 1a plots the scatter diagram of the subsequent 24-h IR against the initial TC intensity, together with the 50th and 95th percentiles of IR, shown as red and black curves. Overall, the IR increases as the intensity increases when the 10-m sustained wind speed is below about 70–80 kt (Fig. 1a), which includes both tropical storms and category-1 hurricanes. This result is consistent with the theoretical studies of Schubert and Hack (1982) and Pendergrass and Willoughby (2009). They showed that greater intensity tends to have higher heating efficiency to intensify the TC vortex because of higher inner-core inertial stability. Since the 95th percentile of IR can represent RI roughly (Kaplan and DeMaria 2003), this result suggests that $V_{\max}$ of 70–80 kt is the most favorable initial TC intensity for RI, consistent with the findings of Kaplan et al. (2010).

The IR tends to decrease with the TC intensity when the storm becomes stronger than 70–80 kt. A possible explanation for this feature is that as an intensifying TC approaches its MPI, the higher heating efficiency is mostly offset by the energy dissipation due to surface friction, which is proportional to the cubic power of the surface wind speed, giving the intensity to asymptote to the MPI despite the greater efficiency of eyewall heating (Pendergrass and Willoughby 2009). Kaplan et al. (2010) supposed that TCs of this intensity are both sufficiently well organized and relatively far from their MPI, making it a relatively favorable intensity for a TC to undergo RI.

[1] This means that the AR34 was defined as the radius of 34-kt surface wind in only one quadrant if the radii were zero in all of the other three quadrants, or the average of the two radii if the radii were zero in the other two quadrants, or the average of three radii if the fourth radius was zero, or the average of the all four radii if none of them was zero. If none of the radii was greater than zero, then the AR34 was zero.

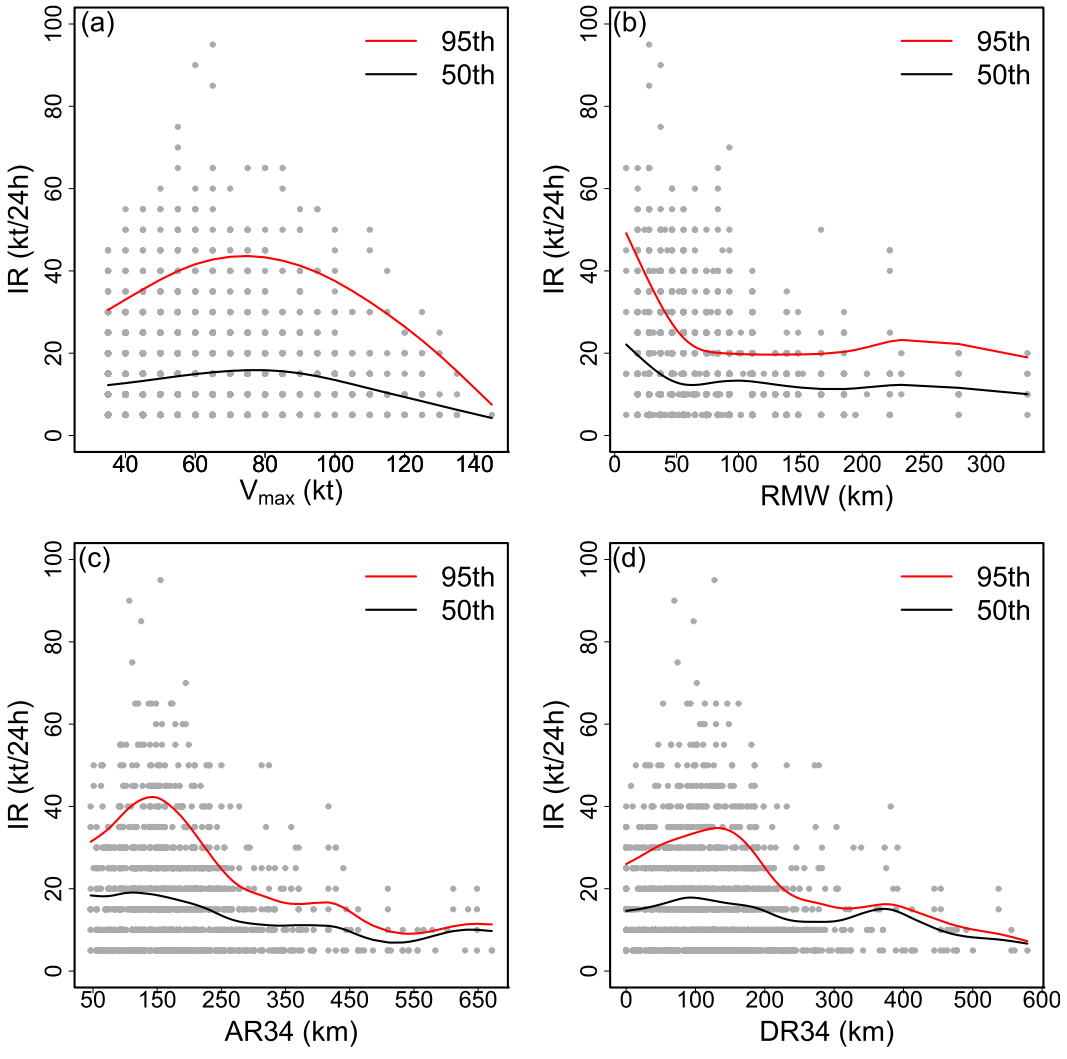

FIG. 1. Scatter diagrams of the subsequent 24-h IR against (a) storm intensity (V_{max} in terms of the max 1-min-mean sustained 10-m wind speed), (b) RMW, (c) AR34, and (d) DR34 (=AR34 − RMW). Red and black curves are the 95th and 50th percentiles of the IR for given storm intensity in (a) and various size parameters in (b)–(d), respectively.

The above dependence of IR on the initial TC intensity can be understood based on the simplified dynamical system for TC intensity prediction developed by DeMaria (2009). The dynamical system was an analogy with the so-called logistic growth equation (LGE) commonly used to model population growth and mathematically is shown in his Eq. (3) and is given below

$$\mathrm{IR} = \frac{dV}{dt} = \kappa V - \beta V \left(\frac{V}{V_{\mathrm{mpi}}} \right)^{n}, \tag{4}$$

where the time tendency of the maximum sustained surface winds V, namely the IR, is determined by two terms—a growth term and a term that limits the maximum wind to an upper bound V_{mpi}, which is the MPI in terms of the maximum surface wind speed and can be calculated from the sea surface temperature and atmospheric sounding on the storm track; κ is the time-dependent growth rate; and β and n are positive constants that determine how rapidly and how close the solution for V can come to V_{mpi}. With the regression using historical best-track data, DeMaria (2009) found the values for β and n to be $1/24\,\mathrm{h}^{-1}$ and 2.5, respectively. Based on Eq. (4) and letting $\partial \mathrm{IR}/\partial V = 0$, we can find that IR reaches a maximum value when the storm intensity is around V_{mpir}, given by

$$V|_{\mathrm{mpir}} = V_{\mathrm{mpi}} \left[\frac{\kappa}{(n+1)\beta} \right]^{1/n}. \tag{5}$$

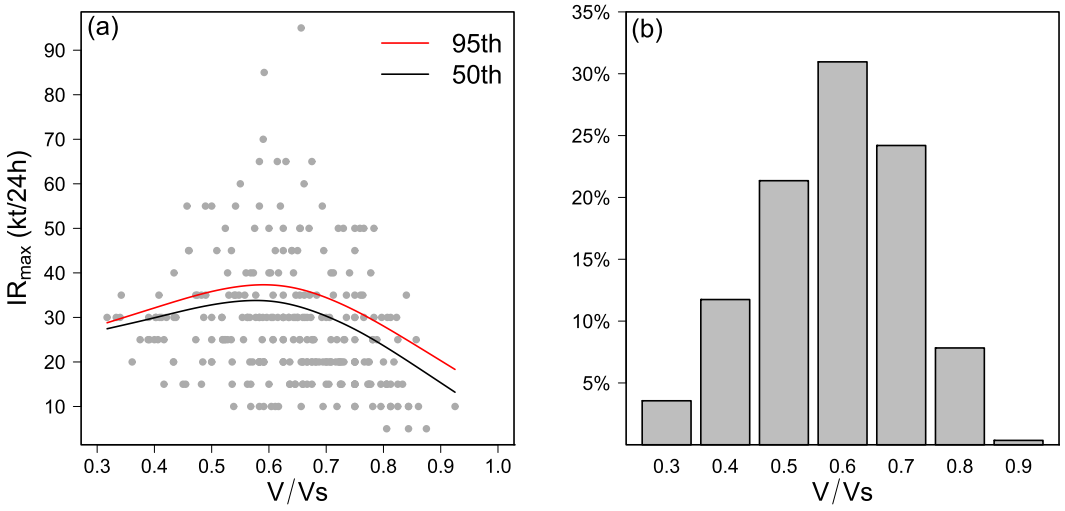

FIG. 2. (a) Scatter diagram of the lifetime max 24-h IR against the average storm intensity during the 24-h IR_{max} period in terms of the max 1-min-mean sustained 10-m wind speed normalized by the lifetime max intensity of the storm (namely V/V_s). The red and black curves are the 95th and 50th percentiles of IR_{max} for the given normalized storm intensity. (b) The frequency distribution of the lifetime IR_{max} as a function of the corresponding normalized storm intensity.

DeMaria (2009) showed that there exists a steady-state intensity V_s, which can be considered to be the real maximum intensity of the storm in given environmental conditions. Namely, letting $dV/dt = 0$ in Eq. (4), we can obtain

$$V_s = V_{\mathrm{mpi}}\left(\frac{\kappa}{\beta}\right)^{1/n}. \tag{6}$$

Using Eq. (6), Eq. (5) can be rewritten as

$$V_{\mathrm{mpir}} = V_s(n+1)^{-1/n} \approx 0.606V_s. \tag{7}$$

Equation (7) suggests that the IR reaches a maximum when the storm is at its intermediate intensity.

Since the dynamical system in Eq. (4) includes the time-dependent coefficients κ and V_{mpi}, we could not calculate the steady-state intensity for each storm from Eq. (6). Here, we use the lifetime maximum intensity of each storm as an estimate for the steady-state intensity V_s. Figure 2a shows the scatter diagram of the lifetime maximum intensification rate IR_{max} for each storm against the corresponding storm intensity V_{mpir} (which is defined as the mean storm intensity during the 24-h period of the IR_{max} for consistency) normalized by its steady-state intensity. In Fig. 2a, we also show the 95th and 50th percentiles of the IR_{max}. We can see that a peak exists in IR_{max} as V/V_s is around 0.6, consistent with the intensity dependence of the IR on the storm intensity, as shown in Fig. 1a in the observations. Figure 2b shows the frequency distribution of the storm V_{mpir} normalized by V_s at the IR_{max} for all cases. It demonstrates that the majority of TCs (over 76%) reached their lifetime maximum IRs when their normalized intensity (V/V_s) was between 0.5 and 0.7, in agreement with that predicted from Eq. (7).

b. Dependence on storm size

Figures 1b–d show the scatter diagrams of the subsequent 24-h IR against the size parameters RMW, AR34, and DR34. The IR is negatively correlated with RMW, which is consistent with the results of Carrasco et al. (2014), with a linear correlation coefficient of −0.173, which is slightly smaller than theirs (−0.22) mainly because of our larger sample size. This negative correlation can be much more clearly seen from the smoothed curve of the 95th percentile for the RMW, which is less than about 150 km (Fig. 1b). In particular, a sharp increase in IR occurred when the RMW decreases from about 60 to 20 km for both the median and 95th percentiles for the RMW. This demonstrates that RI is hard to achieve for TCs with relatively large inner-core sizes. Note that cases for the RMW greater than 150 km are not representative because of the small sample size. This result supports earlier theoretical studies since smaller RMW generally implies larger inner-core inertial stability and thus higher efficiency of eyewall heating to intensify the storm (Schubert and Hack 1982; Pendergrass and Willoughby 2009).

The outer-core size AR34 shows an overall negative correlation with IR (Fig. 1c) very similar to the inner-core size RMW (Fig. 1b), in agreement with the findings of Carrasco et al. (2014). The AR34 has a higher negative correlation with the subsequent IR than the RMW,

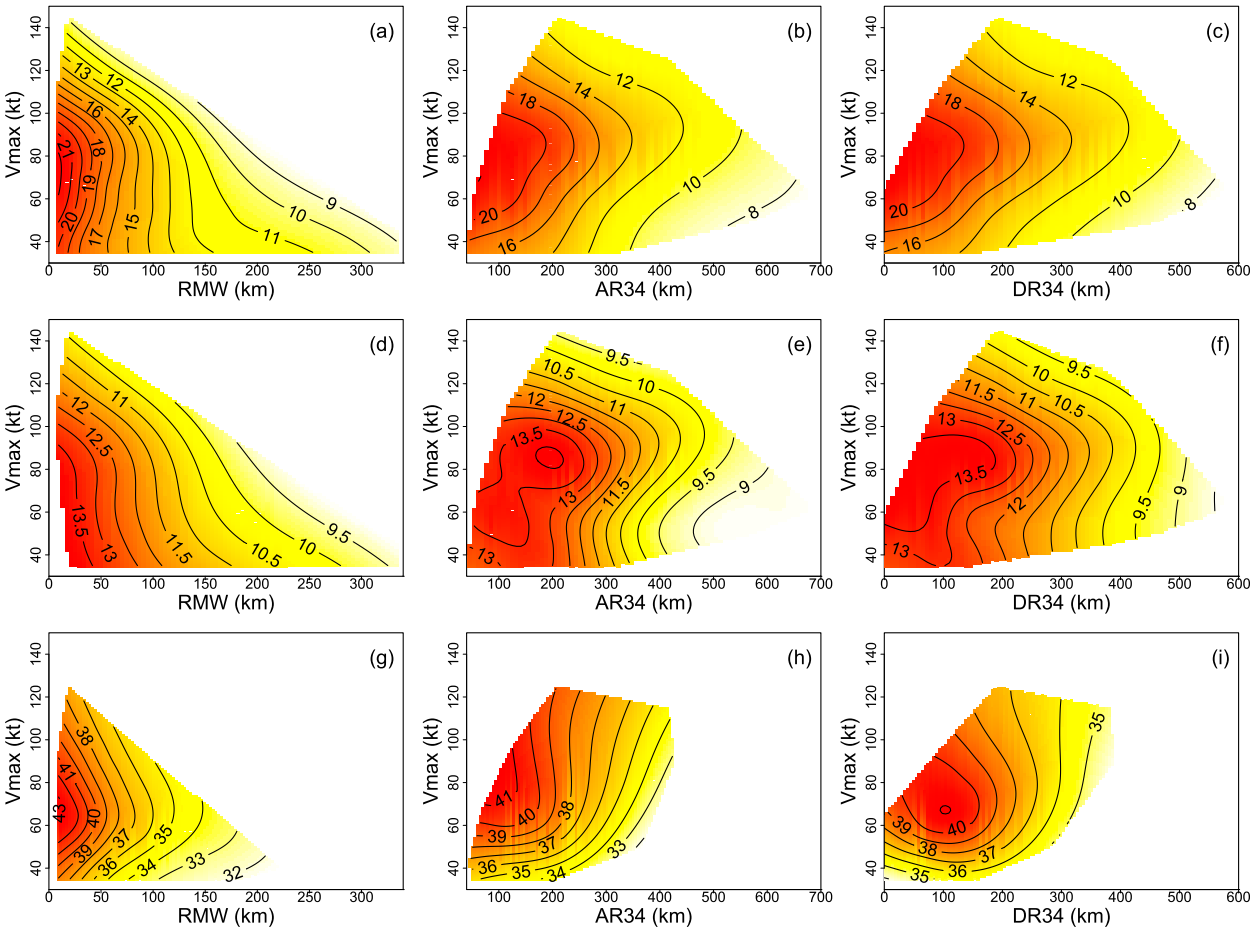

FIG. 3. The smoothed subsequent 24-h IR as a function of V_{max} and (a) RMW, (b) AR34, and (c) DR34 (=AR34 − RMW) using regression spline fitting as described in section 2. (d)–(f) As in (a)–(c), but for non-RI cases. (g)–(i) As in (a)–(c), but for RI cases.

with a correlation coefficient of −0.194 (vs −0.173 for RMW, both significant at the 95% confidence level and above). Note that this is slightly different from the results of Carrasco et al. (2014), who found that the RMW is more important than the AR34 for TC IR. This inconsistency might suggest that both RMW and AR34 are important to TC IR. Note also that unlike the effect of RMW, the effect of AR34 on IR shows an optimal value where the response of IR reaches a maximum when AR34 is around 150 km (Fig. 1c). The increasing trend of IR with the increase in AR34 for AR34 less than 150 km might be largely due to the positive correlation between AR34 and TC intensity for initially weak TCs. Note that AR34 is zero for a TC just reaching its tropical storm intensity.

The decreasing trend of IR with the increase in AR34 for AR34 larger than 150 km suggests that smaller outer-core size or compact structure favors RI, as also shown in Chen et al. (2011). Note that for a given intensity and RMW, a larger AR34 indicates a slow decaying rate for the tangential wind with radius outside the RMW. This result thus implies that slow-decaying tangential wind outside the RMW is unfavorable for RI. This is consistent with the findings of Rogers et al. (2013), who showed that slow-decaying outer-core wind is unfavorable for intensification.

Figure 1d shows the scatter diagram for IR against DR34, an alternative parameter to measure the outer-core size in this study. The 95th percentile shows a decreasing trend of IR with increasing DR34 when DR34 is larger than about 100 km, while a small increasing trend is found for DR34 less than about 100 km. Note that large IR (or RI) occurs mainly for DR34 between 50 and 150 km. The dependence of IR on DR34 is very similar to that on AR34 and results from similar reasons, as discussed above for AR34. Note that the results above are not in conflict with previous findings that the inner-core intensity and outer-core strength of a TC are highly independent (Weatherford and Gray 1988; Kimball and Mulekar 2004) because we focused on IR not the

simultaneous relationship between the inner-core intensity and outer-core strength. In addition, we used DR34 as an approximation of the decaying rate of tangential wind with radius, which is not a direct measure of the outer-core strength.

c. Combined effect of intensity and size

To further examine the combined effect of the initial intensity and size, the thin plate smoothing spline fitting described in section 2 was employed to present the functional relationships of the subsequent 24-h IR, non-RI, and RI with the TC intensity and size parameters (Fig. 3). Note that the area with data indicates the possible coexistence of the size parameter for a given intensity. The fitted surface can reflect the majority of the joint parameter space. From Figs. 3a, 3d, and 3g, we can see that IR increases as the RMW decreases and relatively high IR (thus RI) occurs for TCs with intensity predominantly between 40 and 100 kt. The highest IR occurs when V_{max} is around 80 kt and RMW is 20 km for all RI and non-RI cases (Figs. 3a,d) while the highest RI occurs when V_{max} is around 70 kt. Comparing Fig. 3d with 3g, we can see that the parameter space in V_{max} and RMW for RI is much smaller than that for non-RI, suggesting that RI can occur only in a small parameter space of moderate intensity and small inner-core size. Note that TCs with too large RMW (≥220 km) still have a chance to intensify but rarely intensify rapidly.

Figure 3b suggests that IR is relatively high when V_{max} is between 60 and 90 kt and AR34 is between 50 and 100 km. Note that only when V_{max} is greater than 34 kt does AR34 have values by definition. Similar to the results for RMW, RI (Fig. 3h) occurs in a much smaller parameter space in V_{max} and AR34 than does non-RI (Fig. 3e). The highest RI appears when V_{max} is around 70–80 kt and AR34 is around 100 km. A very similar pattern can be seen for the parameter space in V_{max} and DR34, as shown in Figs. 3c, 3f, and 3i. A major difference is that there exists a maximum center in the parameter space in V_{max} and DR34 (Fig. 3i), where V_{max} is around 60–80 kt and DR34 is in the range of 50–150 km. As was mentioned earlier, this is mainly a result of the fact that small DR34 is often related to relatively weak TCs, which are unfavorable for RI. On the other hand, large DR34 implies a large outer-core size and a slow decaying rate of tangential wind with radius, thus having relatively high inertial stability outside the RMW. The high inertial stability outside the RMW could reduce the boundary layer inflow, reducing the mass flux into the eyewall and suppressing eyewall convection. This is unfavorable for RI, as was also discussed in Rogers et al. (2013). In addition, strong outer-core tangential winds may also contribute to active spiral rainbands through enhanced surface fluxes. Latent heat released in spiral rainbands could increase the TC size but reduces the TC IR (Xu and Wang 2010a,b).

d. Frequency distribution

In addition to IR, it is also interesting to examine the frequency of occurrence of all intensifying TCs, as well as non-RI and RI TCs, in the parameter space of V_{max}–RMW, V_{max}–AR34, and V_{max}–DR34, respectively (Fig. 4). We can see that most of the intensifying cases occur for TCs with RMW between 40 and 100 km and intensity between 34 and 80 kt (Fig. 4a). The distribution of non-RI cases in the V_{max}–RMW space (Fig. 4d) is very similar to that of all intensifying cases (Fig. 4a). However, the RI cases show higher frequency with the RMW between 60 and 100 km for weak TCs ($V_{max} \leq$ 40–60 kt), while with the RMW is less than about 60 km for medium-intensity TCs with V_{max} between 60 and 80 kt (Fig. 4g). The RI frequency of occurrence has a decreasing trend for intense TCs with V_{max} greater than 80 kt. Note that for intensifying TCs with V_{max} less than 80 kt, there exists an increasing trend in the frequency of occurrence as the RMW decreases and V_{max} increases. This is mainly a result of the eyewall contraction as a TC intensifies. Interestingly, the distribution of frequency of occurrence in the V_{max}–RMW space is different from those for IR cases shown in Fig. 3. This is mainly due to the fact that many TCs intensify or intensify rapidly but could not reach their MPI because of other detrimental effects, such as the environmental vertical wind shear (Wang and Wu 2004).

The distribution of frequency of occurrence in the V_{max}–AR34 space is quite different from that in the V_{max}–RMW space. As AR34 increases, the maximum in the frequency of occurrence increases with the increase in V_{max} for all intensifying, non-RI, and RI cases (Figs. 4b,e,h). This is mainly a result of the increase in AR34 as a TC intensifies. Note that RI cases occur mostly for AR34 of less than 100 km for weak TCs while for AR34 between 50 and 200 km for moderate and intense TCs (Fig. 4e). The distribution of frequency of occurrence in the V_{max}–DR34 space (Figs. 4c,f,i) shows a similar pattern to that in the V_{max}–AR34 space (Figs. 4b,e,h). Namely, as the DR34 increases, the maximum in the frequency of occurrence of intensifying, non-RI, and RI cases increases with the increase in V_{max}. This implies that, as is the case for AR34, DR34 increases as a TC intensifies, although a maximum in IR occurs for AR34 and DR34 between 50 and 200 km (Figs. 1c,d).

4. Summary

In this study, the dependence of the subsequent 24-h IR (and RI) on TC initial intensity and structure

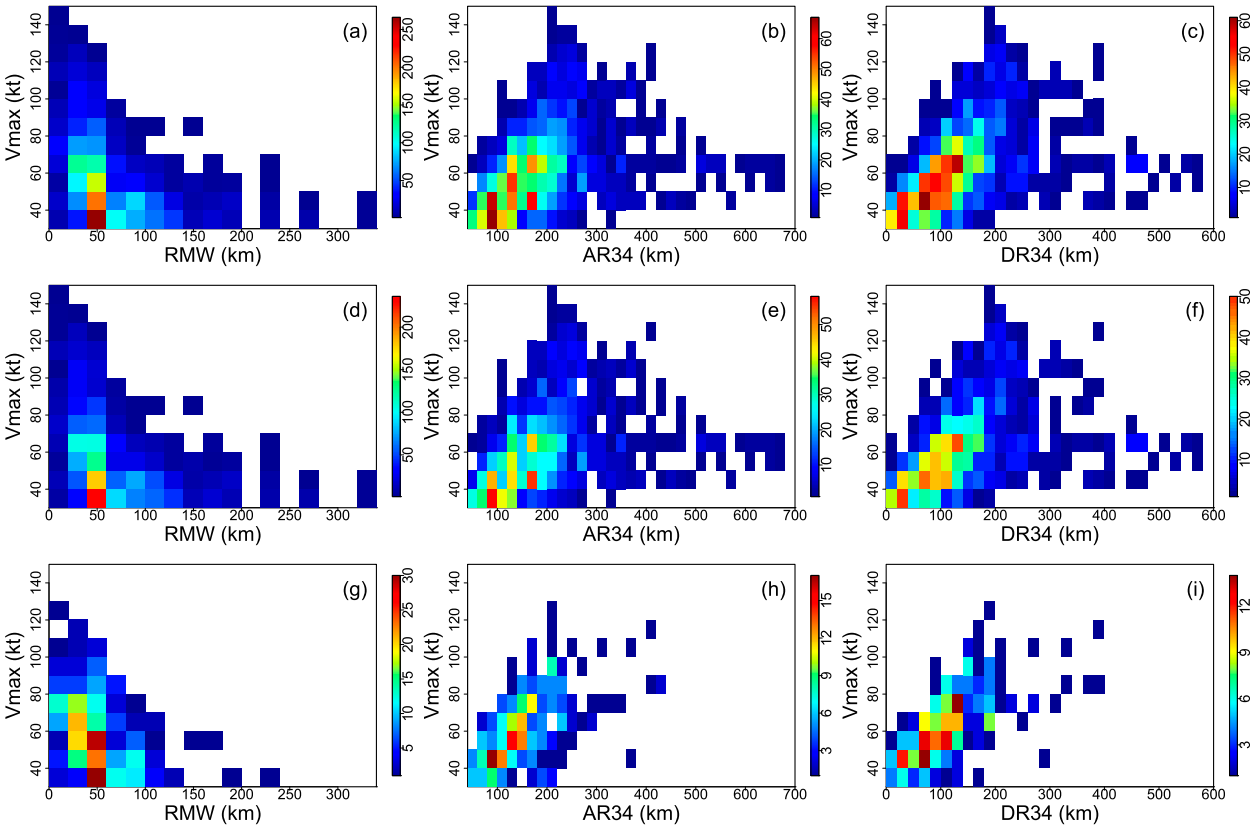

FIG. 4. Distributions of numbers of (top) total intensification TCs, (middle) non-RI TCs [with IR less than 30 kt (24 h)$^{-1}$], and (bottom) RI TCs.

(including the inner- and outer-core sizes, and outer-core wind shape) was analyzed based on the best-track and the extended-best-track datasets for North Atlantic TCs during 1988–2012. The results confirm the previous finding of DeMaria et al. (2005), DeMaria (2009), and Kaplan et al. (2010) that the IR depends strongly on the initial storm intensity. The IR is negatively correlated with the storm size in terms of the RMW and AR34, as well as the wind skirt parameter DR34 (Table 1). The IR is positively correlated with the initial storm intensity when V_{max} is less than 80 kt, while it is negatively correlated with the initial storm intensity when V_{max} is larger than 80 kt (Table 1).

The turning point for V_{max} was explained as a balance between the potential intensification and the MPI of the TC. The initial increase in IR with the storm intensity is due to the increasing efficiency of the intensification to eyewall heating because of the increasing inner-core inertial stability. The decreasing trend of IR with the increasing TC intensity when the storm becomes stronger than 80 kt is a result of the offset of the increasing heating efficiency by the energy dissipation due to

TABLE 1. List of sample sizes, TC cases, and correlation coefficients between TC IR and the storm intensity of various size parameters. The p values indicate the statistical confidence for the corresponding correlation coefficient. Because of the sample-size dependency [p value (S)] with all of the 6-h data, p values based on the degrees of freedom with only TC cases are shown as p value (C). All correlations are significant above the 90% confidence level for p value (C). Note that if the TC days are used to estimate the degrees of freedom, all correlations are significant above the 98% confidence level (not shown), suggesting the robustness of the correlations.

	$34 \le V_{max} \le 80$ kt	$V_{max} > 80$ kt	RMW	AR34	DR34
Sample size	2300	334	2408	1875	1768
TC cases	281	71	258	214	208
Correlation coef	0.13	−0.26	−0.17	−0.18	−0.13
p value (S)	1.74×10^{-10}	2.06×10^{-6}	2.20×10^{-16}	1.80×10^{-14}	6.73×10^{-8}
p value (C)	0.026	0.031	0.005	0.010	0.066

surface friction, which is proportional to the cubic power of the surface wind speed. As a result, the intensity eventually approaches the MPI despite the greater efficiency of eyewall heating. Therefore, TCs of this intensity are both sufficiently well organized and relatively far from their MPI and favorable for RI, as suggested by Kaplan et al. (2010). The simple dynamical system for TC intensity prediction developed by DeMaria (2009) is used to provide a theoretical basis for this intensity dependence of IR, which predicts that both the maximum and the majority of the lifetime maximum IR cases occur when a TC is at its lifetime intermediate intensity.

The general increase in IR with the decrease in the RMW results mainly from higher inertial stability for smaller RMW for a given TC intensity. In particular, RI rarely occurs for TCs with an RMW larger than 220 km. The IR shows a maximum response when AR34 is around 150 km, indicating the dominant effect of TC intensity for AR34 less than 150 km while a negative effect of AR34 on IR for AR34 larger than 150 km is found. Since for a given intensity and RMW, a larger AR34 indicates slower decaying rate of tangential wind with the radius outside the RMW, the results suggest that slow-decaying outer-core wind speed with radius is unfavorable for TC RI. A similar dependence of IR on DR34 is also true since DR34 is highly correlated with AR34 by definition. We found that large IR (or RI) occurs mainly for DR34 between 50 and 150 km.

In the combined size–intensity parameter space, the highest IR occurs for V_{max} around 70–80 kt, RMW = 10–20 km, and AR34 = DR34 = 150 km. The high frequency of occurrence of intensifying TCs occurs for $V_{max} \leq 80$ kt and RMW between 20 and 60 km, AR34 $\leq$ 200 km, and DR34 $\leq$ 150 km. RI tends to occur in a relatively small parameter space in storm intensity and size.

Results from this study strongly suggest that both intensity and size parameters should be considered as good predictors in operational statistical TC intensity prediction models. Although previous studies have revealed the strong dependence of IR on TC initial intensity and the initial storm intensity has also been used as a predictor in some operational statistical intensity prediction schemes [e.g., SHIPS and LGE intensity prediction model (LGEM)], in this study we have further confirmed such a dependence with longer data records and also provided a theoretical basis for interpreting the dependence. As noted by Carrasco et al. (2014), the storm size parameters have not been presently considered in operational prediction schemes. This might be partly due to the lack of a systematic analysis on the dependency of TC intensification on storm structure based on observations and partly due to the lack of accurate measurements of storm size (structure) parameters from observations. This study, together with the work of Carrasco et al. (2014), may serve as a first step to fill this gap toward improved TC intensity forecasts by introducing storm intensity and size parameters into operational statistical intensity prediction schemes.

Acknowledgments. This study has been supported in part by the National Natural Science Foundation of China under Grants 41130964 and 41105041 and in part by the NSF Grant AGS-1326524, as well as a JAMSTEC grant to the University of Hawai'i at Mānoa. The official best-track data for Atlantic TCs, known as HURDAT2, were downloaded from the National Hurricane Center (NHC; http://www.nhc.noaa.gov/data/#hurdat) and the Extended Best-Track (EBT) data for North Atlantic TCs during 1988–2012 were downloaded from the Colorado State University (CSU) website (http://rammb.cira.colostate.edu/research/tropical_cyclones/tc_extended_best_track_dataset/).

REFERENCES

Carrasco, C., C. Landsea, and Y. Lin, 2014: The influence of tropical cyclone size on its intensification. *Wea. Forecasting,* **29,** 582–590, doi:10.1175/WAF-D-13-00092.1.

Chen, D. Y.-C., K. K.-W. Chang, and C.-S. Lee, 2011: Some implications of core regime wind structures in western North Pacific tropical cyclones. *Wea. Forecasting,* **26,** 61–75, doi:10.1175/2010WAF2222420.1.

DeMaria, M., 2009: A simplified dynamical system for tropical cyclone intensity prediction. *Mon. Wea. Rev.,* **137,** 68–82, doi:10.1175/2008MWR2513.1.

——, and J. Kaplan, 1999: An updated Statistical Hurricane Intensity Prediction Scheme (SHIPS) for the Atlantic and eastern North Pacific basins. *Wea. Forecasting,* **14,** 326–337, doi:10.1175/1520-0434(1999)014<0326:AUSHIP>2.0.CO;2.

——, M. Mainelli, L. K. Shay, J. A. Knaff, and J. Kaplan, 2005: Further improvements to the Statistical Hurricane Intensity Prediction Scheme (SHIPS). *Wea. Forecasting,* **20,** 531–543, doi:10.1175/WAF862.1.

Demuth, J. L., M. DeMaria, and J. A. Knaff, 2006: Improvement of Advanced Microwave Sounding Unit tropical cyclone intensity and size estimation algorithms. *J. Appl. Meteor. Climatol.,* **45,** 1573–1581, doi:10.1175/JAM2429.1.

Elsberry, L. E., T. D. B. Lambert, and M. A. Boothe, 2007: Accuracy of Atlantic and eastern North Pacific tropical cyclone intensity forecast guidance. *Wea. Forecasting,* **22,** 747–762, doi:10.1175/WAF1015.1.

——, L.-S. Chen, J. Davidson, R. Rogers, Y. Wang, and L. Wu, 2013: Advances in understanding and forecasting rapidly changing phenomena in tropical cyclones. *Trop. Cyclone Res. Rev.,* **2,** 13–24.

Gray, W. M., 1979: Tropical cyclone intensity determination through upper-tropospheric aircraft reconnaissance. *Bull. Amer. Meteor. Soc.,* **60,** 1069–1074, doi:10.1175/1520-0477(1979)060<1069:TCIDTU>2.0.CO;2.

Green, P. J., and B. W. Silverman, 1994: *Nonparametric Region and Generalized Linear Models: A Roughness Penalty Approach.* Chapman and Hall, 182 pp.

Kaplan, J., and M. DeMaria, 2003: Large-scale characteristics of rapidly intensifying tropical cyclones in the North Atlantic basin. *Wea. Forecasting,* **18,** 1093–1108, doi:10.1175/1520-0434(2003)018<1093:LCORIT>2.0.CO;2.

——, ——, and J. A. Knaff, 2010: A revised tropical cyclone rapid intensification index for the Atlantic and eastern North Pacific basins. *Wea. Forecasting,* **25,** 220–241, doi:10.1175/2009WAF2222280.1.

Kimball, S. K., and M. S. Mulekar, 2004: A 15-year climatology of North Atlantic tropical cyclones. Part I: Size parameters. *J. Climate,* **17,** 3555–3575, doi:10.1175/1520-0442(2004)017<3555:AYCONA>2.0.CO;2.

Merrill, R. T., 1984: A comparison of large and small tropical cyclones. *Mon. Wea. Rev.,* **112,** 1408–1418, doi:10.1175/1520-0493(1984)112<1408:ACOLAS>2.0.CO;2.

Pendergrass, A. G., and H. E. Willoughby, 2009: Diabatically induced secondary flows in tropical cyclones. Part I: Quasi-steady forcing. *Mon. Wea. Rev.,* **137,** 805–821, doi:10.1175/2008MWR2657.1.

Rogers, R., P. Reasor, and S. Lorsolo, 2013: Airborne Doppler observations of the inner-core structural differences between intensifying and steady-state tropical cyclones. *Mon. Wea. Rev.,* **141,** 2970–2991, doi:10.1175/MWR-D-12-00357.1.

Schubert W. H., and J. J. Hack, 1982: Inertial stability and tropical cyclone development. *J. Atmos. Sci.,* **39,** 1687–1697, doi:10.1175/1520-0469(1982)039<1687:ISATCD>2.0.CO.

Shapiro, L. J., and H. E. Willoughby, 1982: The response of balanced hurricanes to local sources of heat and momentum. *J. Atmos. Sci.,* **39,** 378–394, doi:10.1175/1520-0469(1982)039<0378:TROBHT>2.0.CO;2.

Vigh, J. L., and W. H. Schubert, 2009: Rapid development of the tropical cyclone warm core. *J. Atmos. Sci.,* **66,** 3335–3350, doi:10.1175/2009JAS3092.1.

Wang, Y., and C.-C. Wu, 2004: Current understanding of tropical cyclone structure and intensity changes—A review. *Meteor. Atmos. Phys.,* **87,** 257–278, doi:10.1007/s00703-003-0055-6.

Weatherford, C. L., and W. M. Gray, 1988: Typhoon structure as revealed by aircraft reconnaissance. Part I: Data analysis and climatology. *Mon. Wea. Rev.,* **116,** 1032–1043, doi:10.1175/1520-0493(1988)116<1032:TSARBA>2.0.CO;2.

Xu, J., and Y. Wang, 2010a: Sensitivity of the simulated tropical cyclone inner-core size to the initial vortex size. *Mon. Wea. Rev.,* **138,** 4135–4157, doi:10.1175/2010MWR3335.1.

——, and ——, 2010b: Sensitivity of tropical cyclone inner core size and intensity to the radial distribution of surface entropy flux. *J. Atmos. Sci.,* **67,** 1831–1852, doi:10.1175/2010JAS3387.1.